Proceedings of the IASS Annual Symposium 2016
"Spatial Structures in the 21st Century"
26–30 September, 2016, Tokyo, Japan
K. Kawaguchi, M. Ohsaki, T. Takeuchi (eds.)

Topology optimization of supporting structures for seismic response reduction of spatial structures

Yuji MIYAZU*, Makoto OHSAKI[a], Seita TSUDA[b]

* Department of Architecture, Hiroshima University
Higashi-Hiroshima 739-8527, Japan
miyazu@hiroshima-u.ac.jp

[a] Kyoto University
[b] Okayama Prefectural University

Abstract

A flexible supporting structures reducing seismic responses of two types of spatial structures, an arch and a latticed dome, are proposed. The supporting structures of the arch and the latticed dome are modeled as two- and three-dimensional truss structures, respectively, and their topology and cross-sectional areas are optimized solving nonlinear programming problems. The optimization problem of the arch is divided into two small optimization problems to obtain the optimal solution efficiently. It is demonstrated through time-history response analysis that the flexible supporting structure can reduce the seismic response of the roof structures, and installing viscous dampers into the supporting structure is effective to further reduction of the responses.

Keywords: arch, latticed dome, flexible supporting structure, topology optimization, seismic response

1. Introduction

Various seismic response control systems, for example, stiff seismic design, base isolation, and passive energy dissipation system have been proposed to reduce seismic damage of building structures. Some of them are effective also to spatial structures such as arches, domes and shells; however, it is rather difficult to control seismic response of spatial structures because several modes should be considered in the process of response evaluation.

The main seismic damages of spatial structures caused by recent earthquakes are the fall of non-structural components such as ceilings and hanging equipments, and the damage at the connection between the roof and the supporting structure. One of the methods to control these damages is to reduce the acceleration response and the inertia force of the roof structure. The previous study by Ohsaki et al. [1] shows that using the flexibility of a base structure is effective in reducing roof displacement and acceleration of a building frame. Miyazu et al. [2] show that the normal response of the roof of an arch can be reduced by flexible supporting structures obtained through topology optimization methods. In this study, we apply the concept of the flexible structure to the supporting structures of two types of spatial structures: an arch and a latticed dome, and we optimize the topology and the shape of the supporting structures.

The arch and the latticed dome are modeled as two- and three-dimensional structures, respectively, and the topology, the shape, and the cross-sectional areas of the supporting structures modeled as pin-jointed trusses are optimized using a nonlinear programming approach. The acceleration response in the normal direction and the inertia force of the roof structures evaluated by the complete quadratic combination (CQC) method are minimized under constraints in stiffness under self-weight. It is shown in numerical study that the flexible supports reducing roof responses are successfully generated by the proposed optimization method. Effectiveness of installing viscous dampers into the flexible supporting structure is also demonstrated through time-history response analyses.

2. Flexible supporting structure for arch

2.1 Overview of flexible support for arch

In an arch supported by conventional stiff structures, as shown in Fig. 1(a), it is known that the normal directional response is excited in the roof structure even when the arch is subjected only to horizontal seismic ground motions. Since the normal response of the roof causes the buckling of roof members and falling of non-structural members [3], reducing the normal response of the roof structure is one of the important point in the seismic design of arches.

Figure 1 (b) shows the concept of the reduction of the normal directional response by utilizing the flexibility of the supporting structure. By using the supporting structures whose top node moves mainly in the tangential direction of the roof, as shown by thick arrows in Fig. 1(b), it is expected that the normal directional response of the roof is reduced.

In our previous study [2], the flexible supporting structure for an arch is generated through two steps of static and dynamic topology optimization. In this study, we optimize not only the topology but also the shape of the supporting structure in the dynamic optimization problem to obtain better solutions. In Section 2.2, the results of the static optimization are summarized for completeness of the paper.

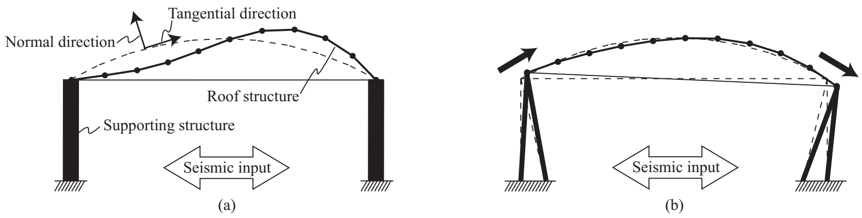

Figure 1: (a) An arch with stiff supporting structures; (b) an arch with flexible supporting structures.

2.2 Static optimization problem

The static optimization problem for a supporting structure is solved to obtain the supporting structure whose top node moves in the diagonal direction under lateral load as shown in Fig 2(a). The conventional ground structure approach is used for topology optimization.

The ground structure has 10 nodes including supports and 29 truss members which are not connected at their intersections without nodes. The mass of 4000 kg is attached at node 10 to represent the mass of a roof structure. The weight of the truss members is ignored.

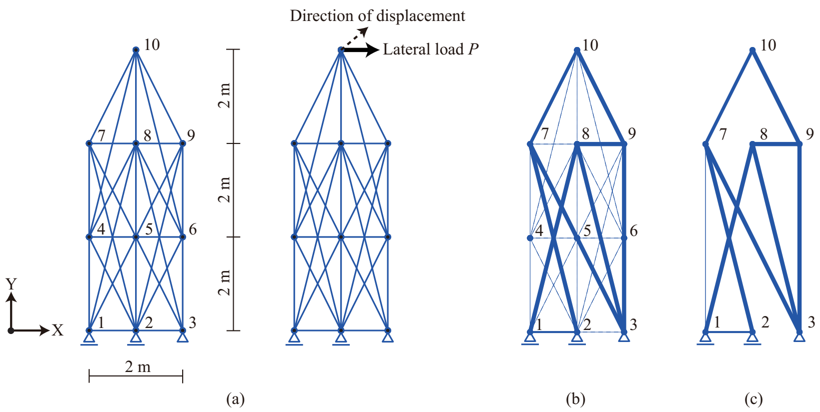

Figure 2: (a) Ground structure for static topology optimization; (b) topology of the optimal solution; (c) final topology of the optimal solution.

Let d_{hv} and d_{hh} denote the displacement in the Y- and X- directions, respectively, of node 10 under a lateral load P = 7.84 kN, which corresponds to 20 % of weight of the mass at node 10. The objective function to be maximized is formulated as

$$R = \frac{d_{hv}}{d_{hh}} \tag{1}$$

Design variables are the cross-sectional areas of all m (= 29) truss members, which are denoted by a vector $\mathbf{A} = (A_1, \cdots, A_m)$. The lower and the upper bounds of A_i are $A_i^L = 1.0 \times 10^{-6}$ and $A_i^U = 2.0 \times 10^{-3}$ (m^2), respectively. Let d_{gh} and d_{gv} denote the X- and Y- directional displacements, respectively, under self-weight. In order that the supporting structure has enough vertical stiffness and doesn't have too small lateral stiffness, the lower bounds of $d_{gh}^L = -0.012$, $d_{gv}^L = -0.006$, and $d_{hh}^U = 0.06$ (m) are given. The optimization problem called Problem 1 is formulated as follows:

$$\begin{aligned} \text{Problem 1}: \quad & \text{maximize} \quad R(\mathbf{A}) \\ & \text{subject to} \quad d_{gh}(\mathbf{A}) \geq d_{gh}^L \\ & \qquad\qquad\quad d_{gv}(\mathbf{A}) \geq d_{gv}^L \\ & \qquad\qquad\quad d_{hh}(\mathbf{A}) \leq d_{hh}^U \\ & \qquad\qquad\quad A_i^L \leq A_i \leq A_i^U, \ (i = 1, \cdots, m) \end{aligned} \tag{2}$$

After solving Problem 1, we solve the problem called Problem 2 to remove unnecessary members. Problem 2, which minimize the total volume V(**A**) of truss members under displacement constraint, is formulated as follows:

$$\begin{aligned} \text{Problem 2}: \quad & \text{minimize} \quad V(\mathbf{A}) \\ & \text{subject to} \quad d_{gh}(\mathbf{A}) \geq d_{gh}^L \\ & \qquad\qquad\quad d_{gv}(\mathbf{A}) \geq d_{gv}^L \\ & \qquad\qquad\quad d_{hh}(\mathbf{A}) \leq d_{hh}^U \\ & \qquad\qquad\quad R(\mathbf{A}) \geq CR_{opt} \\ & \qquad\qquad\quad A_i^L \leq A_i \leq A_i^U, \ (i = 1, \cdots, m) \end{aligned} \tag{3}$$

where R_{opt} denotes the optimal solution of Problem 1. Note that R_{opt} is multiplied by a coefficient C (= 0.95) to obtain a lower bound to give sufficient large feasible region.

Optimization problems 1 and 2 are solved using the optimization library SNOPT Ver. 7 [4], which uses sequential quadratic programming. A finite difference approach is used to calculate the sensitivity coefficients. The frame analysis software OpenSees [5] is used for structural analysis.

Figure 2(b) shows the best optimal solution with R(**A**) = 0.517 among ten optimal solutions obtained from randomly generated ten different initial solutions. The cross-sectional area of the members indicated by dashed lines have their lower bound. The width of the solid line is proportional to its cross-sectional area. By removing the members with lower bound cross-sectional area and nodes 4, 5, and 6, which are unstable nodes, we obtain final topology with R(**A**) = 0.590 shown in Fig. 2(c). Note that the thin member connecting nodes 1 and 7 can be manufactured as a spring.

2.3 Dynamic optimization problem

In this section, we optimize the cross-sectional area of the thin member and the shape of the supporting structure by solving dynamic optimization problems considering interaction between the roof and the supporting structures. Figure 3 (a) shows an arch with conventional stiff supporting structures. The roof structure consists of ten steel beam members with Young's modulus 2.05×10^5

N/mm^2. The cross-sectional area and second moment of area of the beam are 4.68×10^{-3} m^2 and 7.21×10^{-5} m^4, respectively. The cross-sectional area of the truss members of the supporting structure is 2.0×10^{-3} m^2. Nodes 10 and 20 are connected by tie bar whose cross-sectional area is 1.0×10^{-3} m^2. The mass of 800 kg and 400 kg are attached at nodes 10 to 20 and at the nodes in the supporting structure except for supports, respectively; thus, the total mass of this arch is 13600 kg. We call this arch *stiff-model*.

Figure 3(b) shows the mode shape of the 1st mode of the stiff-model. The natural periods of the 1st and the 2nd modes are 0.369 s and 0.194 s, respectively. It is seen that the deformation of the roof is much larger than that of the supporting structures.

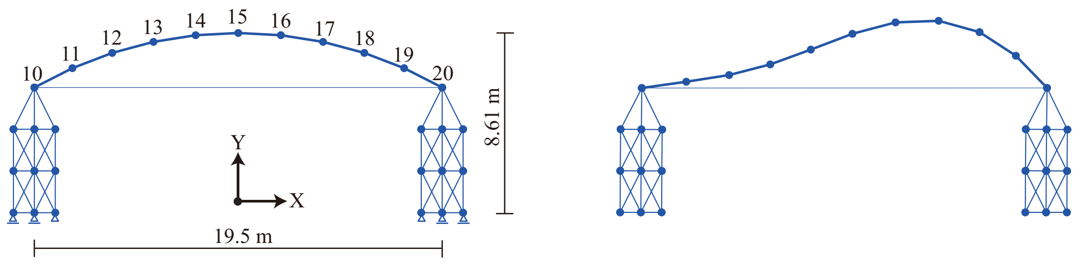

Figure 3: (a) An arch with stiff supporting structures (stiff-model); (b) mode shape of the 1st mode.

Figure 4(a) shows an arch supported by the flexible structure obtained in Section 2.2. The supporting structures are located symmetrically to make the roof moves in the mainly tangential direction as illustrated in Fig. 1(b) under horizontal seismic excitations. The mass of 800 kg is attached at nodes in the supporting structures excluding its supports so that this arch has the same total mass as the stiff-model.

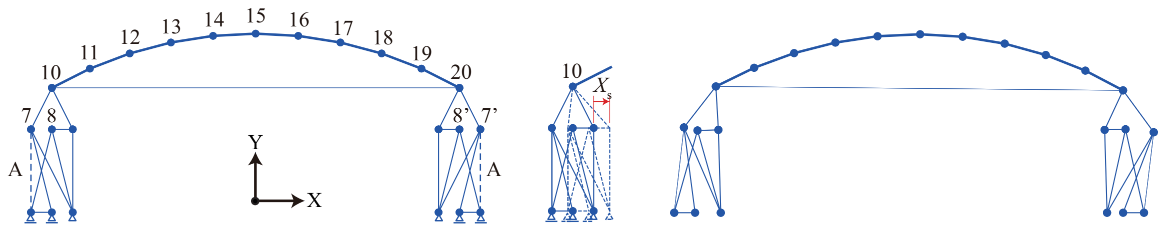

Figure 4: (a) An arch with flexible supporting structures; (b) shape variable X_s of the supporting structure; (c) mode shape of the 1st mode.

Since it has been found through preliminary time-history analysis that the cross-sectional area of member A indicated by dashed lines in Fig. 4(a) plays an important role on the reduction of acceleration response of the roof structure, the cross-sectional area A_A of member A is chosen as a design variable in the following optimization problem. The variable X_s of the supporting structure, which defines the shape of the supporting structure to modify the moving direction of nodes 10 and 20, is illustrated in Fig. 4(b). The objective function to be minimized is evaluated by

$$F(A_A, X_s) = \sqrt{\frac{1}{9}\sum_{i=11}^{19}\left(\ddot{u}_i^n(A_A, X_s)\right)^2} \tag{4}$$

where

$$\ddot{u}_i^n = \sqrt{\sum_{s=1}^{N}\sum_{r=1}^{N}\left(\beta_s\varphi_s^n S_a(T_s, h_s)\rho_{sr}\beta_r\varphi_r^n S_a(T_r, h_r)\right)} \tag{5}$$

$$\rho_{sr} = \frac{8\sqrt{h_s h_r}\left[h_r + \chi^3 h_s + 4\chi h_s h_r (h_r + \chi h_s)\right]\sqrt{\chi}}{\sqrt{(1+4h_s^2)(1+4h_r^2)}\left[(1-\chi^2)^2 + 4h_s h_r \chi (1+\chi^2) + 4(h_s^2 + h_r^2)\chi^2\right]} \tag{6}$$

$$S_a(T_s, h_s) = \frac{1.5}{1+10h_s}\begin{cases} 0.96 + 9.0T_s \quad \text{for} \quad T_s \le 0.16 \\ 2.4 \quad \text{for} \quad 0.16 \le T_s \le 0.864 \\ 2.074 / T_s \quad \text{for} \quad 0.864 \le T_s \end{cases} \tag{7}$$

In Eqs. (4)-(7), $\ddot{u}_i^n$ is the absolute acceleration response in the normal direction of the ith node evaluated by the CQC method [6], ρ_{sr} is the modal-correlation coefficient between the sth and the rth modes, and β_s, h_s, T_s, and φ_s^n are the participation factor, the damping factor, the natural period, and the normal directional component of the sth mode, respectively. The ratio of the natural circular frequencies of the rth mode to that of the sth mode is denoted by χ. Equation (7) defines the design acceleration response spectrum for a middle level earthquake. In the CQC method, the number of modes N is 14, and the modal damping is defined as Rayleigh damping with $h_1 = h_2 = 0.02$.

Let d_{gh} and d_{gv} denote X- and Y- directional displacements of the top node of the left supporting structure under self-weight. In order that the supporting structure has enough vertical stiffness, lower bounds $d_{gh}^L = -0.012$ and $d_{gv}^L = -0.0072$ (m) are assigned. Note that the lower bound d_{gv}^L is relaxed to 120 % of that of Problem 1 to have enough large feasible region. The lower and upper bounds A_{A}^L and A_{A}^U for A_{A} are the same as those for A_i in Section 2.2, and those for X_{s} are $X_{\mathrm{s}}^L = -0.5$ m and $X_{\mathrm{s}}^U = 0.5$ m, respectively. Hence, the optimization problem is formulated as:

$$\begin{aligned} \text{Problem 3}: \quad & \text{minimize} \quad F(A_{\mathrm{A}}, X_{\mathrm{s}}) \\ & \text{subject to} \quad d_{gh}(A_{\mathrm{A}}, X_{\mathrm{s}}) \ge d_{gh}^L \\ & \qquad\qquad\quad d_{gv}(A_{\mathrm{A}}, X_{\mathrm{s}}) \ge d_{gv}^L \\ & \qquad\qquad\quad A_{\mathrm{A}}^L \le A_{\mathrm{A}} \le A_{\mathrm{A}}^U \\ & \qquad\qquad\quad X_{\mathrm{s}}^L \le X_{\mathrm{s}} \le X_{\mathrm{s}}^U \end{aligned} \tag{8}$$

The cross-sectional area A_{A} and the shape variable X_{s} are optimized to find the optimal value $A_{\mathrm{A}} = 8.765 \times 10^{-5}$ m^2 and $X_{\mathrm{s}} = -0.5$ m, respectively. The optimal objective value is 2.51 m/s^2, which is 46 % of that of the stiff-model. This solution is called *flexible-model*. The mode shape of the 1st mode of the flexible-model, illustrated in Fig. 4(c), shows that the large deformation is produced in the supporting structure. The natural periods of the 1st and the 2nd modes are 1.06 s and 0.353 s, which are 2.9 and 1.8 times as large as those of the stiff-model.

2.4 Time-history response

In this section, time-history analyses on the stiff- and the flexible- models are conducted using the software OpenSees to obtain the maximum responses under ground motions. The design acceleration spectrum defined by Eq. (7) is shown in a thick line in Fig. 5(a). Ten seismic ground motions are generated to be compatible with the design response spectrum using random phase. The acceleration response spectra of ten ground motions are shown in thin gray lines in Fig. 5(a). The time increment and the duration of each ground motion are 0.01 s and 60 s, respectively. The time history of one of the ground accelerations is shown in Fig. 5(b).

Figure 6(a) and (b) shows the mean values of the maximum absolute accelerations in the tangential and the normal directions of the nodes. The nodes are identified by X-coordinates. The maximum normal acceleration response among all the nodes of the flexible-model is 44 % of that of the stiff-model; however, since the supporting structure is optimized to move in the tangential direction, the maximum tangential acceleration of the flexible-model increases to 148 % of that of the stiff-model.

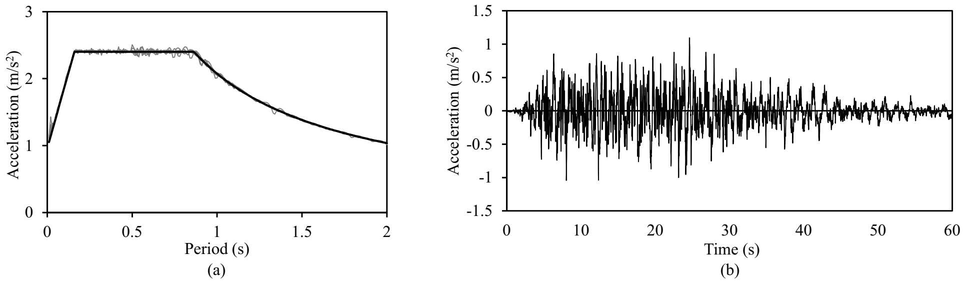

Figure 5: (a) Acceleration response spectra (*h*=0.05). Thick line: design spectrum; thin lines: spectra of ten ground motions.; (b) time history of a ground acceleration.

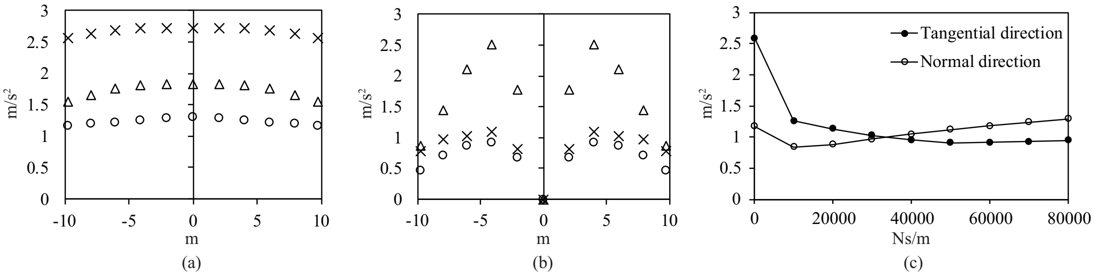

Figure 6: (a) Tangential acceleration response; (b) normal acceleration response (○: Flexible-model with dampers, ×: Flexible-model without dampers, △: Stiff-model); (c) relation between *c* and acceleration responses.

2.5 Installation of viscous dampers

In order to reduce the tangential acceleration increased by the flexible supporting structure, we install viscous dampers between the pairs of nodes 7, 8, and 7’, 8’ in the supporting structure shown in Fig. 4(a), which have large relative displacements under seismic excitations.

Figure 6(c) shows the relation between the damping coefficient c of the dampers and the acceleration responses under the ground motion shown in Fig. 5(b). The ordinate is the norm of acceleration response defined in Eq. (4). It is seen that the dampers with $c \leq$ 50000 Ns/m decrease the tangential acceleration response without increasing the normal acceleration response. The plot of ○ superimposed on Fig. 6(a) and (b) are the results of the flexible-model with the dampers which have c = 10000 Ns/m. It is confirmed that the viscous dampers successfully decrease the tangential acceleration without increase of the normal acceleration.

3. Flexible supporting structure for latticed dome

3.1 Overview of flexible support for latticed dome

The latticed dome considered in this study, shown in Fig. 7, has a roof structure with translational surface, which is supported by four supporting structures at the corners of the roof. In recent earthquakes, failure at the connection between the roof and the supporting structure is one of the main structural damage of domes; therefore, it is assumed that reduction of inertia force of the roof structure is effective to avoid the damage at the connection due to earthquake excitation.

In the case of domes, since the behavior under seismic ground motions is complex because of three dimensional responses, it is difficult to predict the effective deformation characteristics of the supporting structure to reduce the inertia force of the roof. In this study, therefore, we try to optimize the supporting structure through only dynamic optimization problems about roof+supporting structures. Viscous dampers are installed into the optimized supporting structures to further reduce the inertia force of the roof structure. Note that the response under one directional seismic ground motion is considered in this study.

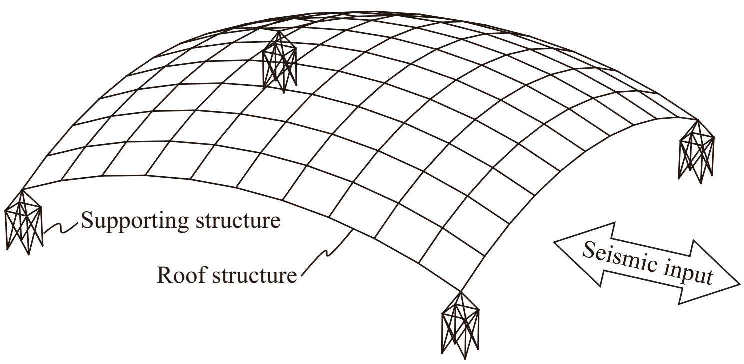

Figure 7: Latticed dome supported by four supporting structures

3.2 Formulation of optimization problem

The structural model of the latticed dome with stiff supporting structures is shown in Fig. 8(a) and (b), where (X, Y, Z) and (u, v, w) indicate the global coordinates and the local coordinates of the roof member, respectively. The roof structure consists of 11 arches in the X- and Y-directions, respectively, and these arches are connected as rigid joints at the intersections. The span of the arch is 19.5 m and the height of the top of the dome from the top of supporting structure is 5.22 m. The cross-sectional area and the second moment of areas with respect to v- and w-axis of the roof members except for the edge arches are 4.678×10^{-3} m^2, 7.210×10^{-5} m^4, and 5.080×10^{-6} m^4, respectively, and those of the members of the edge arches are 1.692×10^{-2} m^2, 9.890×10^{-4} m^4, and 7.660×10^{-5} m^4, respectively. Each supporting structure consists of 20 pin-jointed truss members whose cross-sectional areas are 1.000×10^{-2} m^2. The mass of 1000 kg and 600 kg are attached at the top node and the other nodes, respectively, of the supporting structure, and the mass of 800 kg is attached at the nodes of the roof structure. We call this latticed dome *stiff-model*.

In this section, we optimize the topology and the cross-sectional areas of the supporting structure to reduce the inertia force of the roof structure under X-directional seismic motion. Therefore, the objective function to be minimized is evaluated by

$$F_I = \sqrt{\sum_{s=1}^{N}\sum_{r=1}^{N}\left(\sum_{k=1}^{n} m_k \beta_s \varphi_s^{\mathrm{X}} S_a(T_s, h_s)\rho_{sr}\sum_{k=1}^{n} m_k \beta_r \varphi_r^{\mathrm{X}} S_a(T_r, h_r)\right)} \tag{9}$$

where m_k and φ_s^{X} denote the mass of node k and the X-directional component of the sth mode, respectively. The value of n is 117, which is the number of nodes on the roof structure except for the nodes of the corner. The number of modes N is 50 in this problem. The damping factors $h_1 = h_4 = 0.02$ are used for Rayleigh damping.

Figure 8(c) shows the mode shape of the 1st mode of the stiff-model. It is seen that the deformation of the roof structure is dominant in the model. The natural period of the 1st and the 4th modes are 0.607 s and 0.311 s, respectively. The objective function F_I is 2.02×10^5 N.

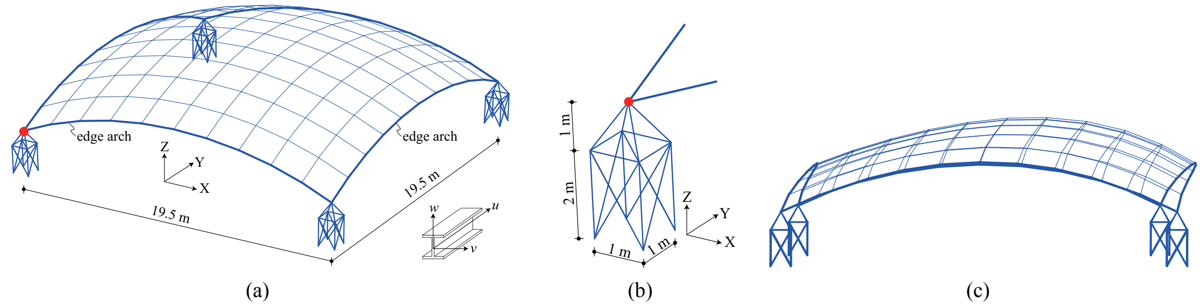

Figure 8: (a) Stiff-model; (b) supporting structure; (c) mode shape of the 1st mode. The width of the line is proportional to the cross-sectional area of the member.

Let d_{gx}, d_{gy}, and d_{gz} denote the X-, Y-, and Z- directional displacement of the top node of the supporting structure, respectively, shown by red filled circle in Figs. 8(a) and (b). The lower bounds $d_{gx}^L = -0.012$, $d_{gy}^L = -0.012$, and $d_{gz}^L = -0.006$ (m) are given to each displacement to avoid too small stiffness against self-weight. The cross-sectional areas A_i of m (=12) truss members shown in Fig. 9(a) and the variation of locations of the nodes of the supporting structure shown by red arrows in Fig. 9(b) are chosen as design variables, which are denoted by vector $\mathbf{A} = (A_i, \cdots, A_m)$ and scalar X. The lower and the upper bounds of $A_i (i = 1, \cdots, m)$ are $A_i^L = 1.0 \times 10^{-5}$ m^2 and $A_i^U = 1.0 \times 10^{-2}$ m^2, respectively, and those of X are $X^L = -0.5$ m and $X^U = 0.5$ m, respectively. Note that the topology of the supporting structure is symmetry with regard to the axes indicated by red dashes lines in Fig. 9 (a) and (c). We formulate the optimization problem called Problem 4 as follows.

$$
\begin{aligned}
\text{Problem 4}: \quad & \text{minimize} \quad && F_I(\mathbf{A}, X) \\
& \text{subject to} \quad && d_{gx}(\mathbf{A}, X) \geq d_{gx}^L \\
& && d_{gy}(\mathbf{A}, X) \geq d_{gy}^L \\
& && d_{gz}(\mathbf{A}, X) \geq d_{gz}^L \\
& && A_i^L \leq A_i \leq A_i^U, \ (i = 1, \cdots, m) \\
& && X^L \leq X \leq X^U
\end{aligned}
\tag{10}
$$

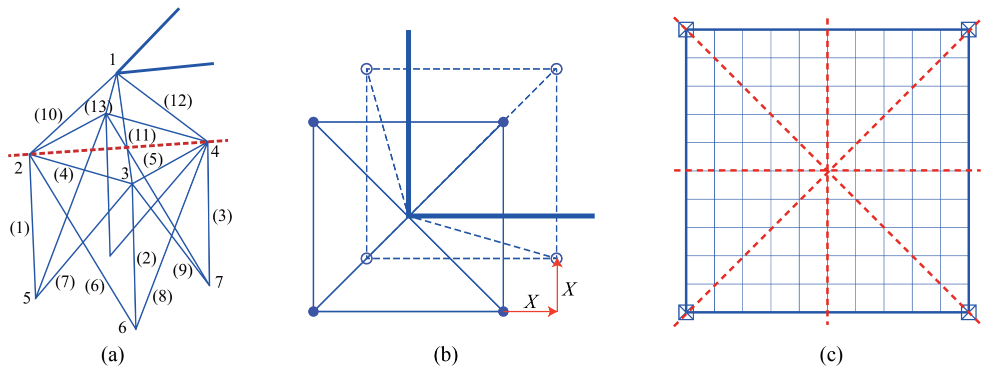

Figure 9: (a) Node and member numbers of the supporting structure; (b) variation of locations of the nodes *X* of the supporting structure; (c) top view of the model.

3.3 Optimization results

Figure 10(a) and (b) show the topology of the optimal solution obtained by solving Problem 4 which has the initial solution with $A_i = A_i^L \ (i = 1, \cdots, m)$ and $X = 0$. The width of the line is proportional to its cross-sectional area, and the members that reach cross-sectional areas of their lower bounds are indicated by dashed lines. The cross-sectional areas of all the members shown by solid lines reach their upper bound. The value of X has its lower bound. The objective function is 1.58×10^5 N, which is about 78 % of that of the stiff-model. Figure 10(c) shows the mode shape of the 2nd mode which has dominant deformation in the X-direction. The natural period is 1.19 s, which is 196 % of the 1st mode natural period of the stiff-model. Note that the 1st mode has the rotational deformation with respect to the Z-axis and the natural period of 1.3 s. It is seen that the in-plane deformation of the roof is smaller and that of the supporting structure is larger compared with those of the stiff-model.

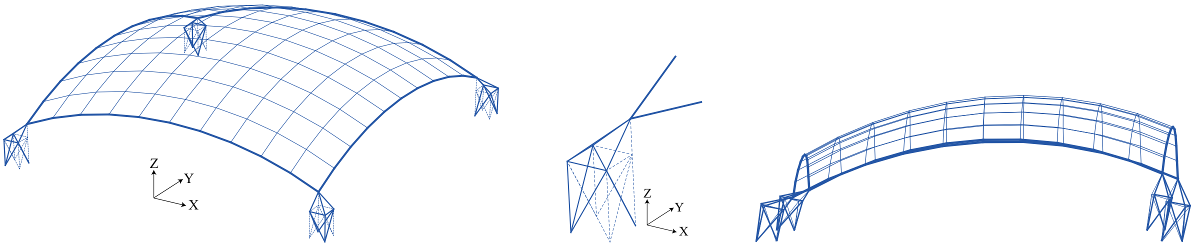

Figure 10: (a) Topology of the optimal solution; (b) supporting structure; (c) the mode shape of the 2nd mode.

Since the supporting structure shown in Fig. 10(b) has unnecessary members and nodes, we remove members 5, 6, 8 and node 4, and replace members 3 and 12 connected to node 4 with one member. By solving Problem 4 with $m = 2$, the cross-sectional areas $A_i\ (i = 1, 2)$ of member 1 and 2 shown in Fig. 11(a) and X are optimized to find optimal values 1.0×10^{-5} m^2 and −0.5 m, respectively. The objective function is 1.24×10^5 N, which is 61 % of that of the stiff-model. We call this model *flexible-model*. The mode shape of the 2nd mode with natural period 1.53 s, shown in Fig. 11(b), is almost the same as Fig. 10(c). Figure 11(c) shows the relation between the objective function F_I and the cross-sectional areas of members 1 and 2, which indicates that small cross-sectional areas of members 1 and 2 are better for reduction of F_I as long as the constraints are satisfied.

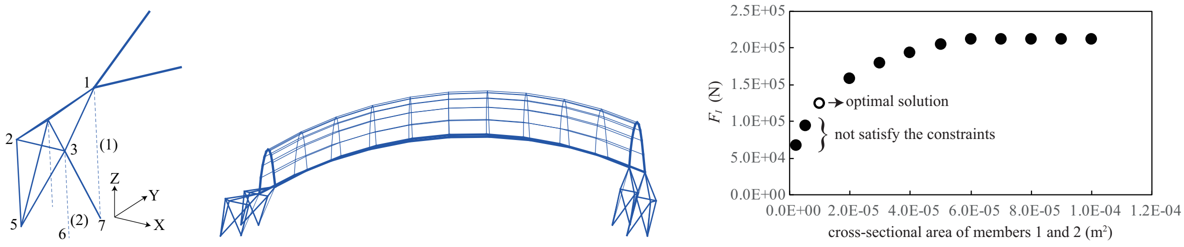

Figure 11: (a) Topology of flexible-model; (b) mode shape of the 2nd mode; (c) relation between the objective function and the cross-sectional area of members 1 and 2.

3.4 Response reduction by viscous dampers

As seen in Fig. 11(b), the relative displacement between nodes 1 and 7 is large in the supporting structure; therefore, installing a viscous damper between the two nodes is assumed to be effective on dissipating a part of seismic input energy. Figure 12(a) shows the relation between the damping coefficient c of the viscous damper with $\overline{F_I}$ which is the mean value of the maximum inertia force of the roof structure in the X-direction, obtained by time history response analysis using ten ground motions. It is confirmed that $\overline{F_I}$ has the smallest value around $c = 2.5 \times 10^5$ Ns/m. Figure 12(b) shows the time history response of the inertia force of the roof structure of the stiff-model and the flexible-model with viscous dampers of $c = 2.5 \times 10^5$ Ns/m. The dampers successfully decrease the inertia force response all over the duration time of the ground motion.

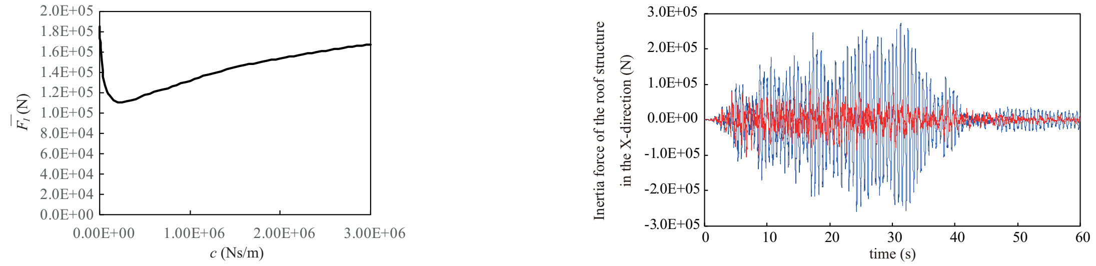

(a) (b)

Figure 12: (a) Relation between c and $\overline{F}_I$; (b) time history of the inertia force of the roof structure. Blue line: stiff-model, red line: flexible-model with viscous dampers.

4. Conclusions

1. The flexible supporting structure of the arch, which makes the roof structure move mainly in the tangential direction to reduce the normal acceleration response of the roof, is successfully generated through two steps of static and dynamic optimization problems.
2. In the latticed dome, the supporting structure which reduces the inertia force of the roof structure under one directional seismic ground motion is obtained by solving dynamic optimization problems.
3. Installing viscous dampers into the flexible supporting structure is very effective to further reduce the seismic response of the roof structures of the arch and the latticed dome.

Acknowledgements

This research is supported by JSPS KAKENHI Grant Number 26630257. The preliminary numerical analysis in Section 3 by Mr. Tetsuto Taguchi, former graduate student of Hiroshima University, is also appreciated.

References

[1] Ohsaki M, Iwatsuki O, Watanabe H. Seismic response of building frames with flexible base optimized for reverse rocking response. *Engineering Structures*, 2014; **74**:170-179.

[2] Miyazu Y, Ohsaki M, Tsuda S. Topology optimization of supporting structure for seismic response reduction of an arch. *SCIENCE CHINA Technological Science*, 2016; **59**:852-861.

[3] Joint Editorial Committee for the Report on the Great East Japan Earthquake Disaster. Report on the Great East Japan Earthquake, Disaster Building Series Volume 3 (in Japanese). Tokyo: Maruzen Publishing Co., 2014. 230–234.

[4] Gill P E, Murray W, Saunders M A. SNOPT: an SQP algorithm for large-scale constrained optimization. *SIAM J Opt*, 2002, **12**: 97–1006.

[5] Open System for Earthquake Engineering Simulation (OpenSees). Pacific Earthquake Engineering Research Center, University of California, Berkeley. 2000.

[6] Wilson E L, Der Kiureghian A, Bayo E P. A replacement for the SRSS method in seismic analysis. *Earthequake Eng Struct Dyn*, 1981, **9**: 187–194.